Applicability of Optical Geometric Differentiation for Time-average Geometric Moiré

M. Ragulskis and L. Saunoriene

Department of Mathematical Research in Systems, Kaunas University of Technology, Studentu 50-222, Kaunas LT-51368, Lithuania

ABSTRACT: Optical experimental method for analysis of derivatives of dynamic displacements from patterns of time-average moiré fringes is proposed in this paper. Derived analytical relationships for one-dimensional optical model are validated for two-dimensional elastic structures performing in-plane vibrations. The fact that digital image filtering techniques are normally required for the identification of time-averaged super-fringes does not lessen the practical value of the proposed method.

KEY WORDS: *geometric differentiation, moiré of moiré, time-average geometric moiré*

NOTATION

δ	Small positive number
ε	Small positive number
φ	Phase of structural vibrations around the state of equilibrium
λ	Pitch of the grating
π	pi
ω	Angular frequency of structural vibrations around the status of equilibrium
$E_{\mathrm{d}}^{\mathrm{super}}$	Envelope function (modulation of super-fringes) of double-exposure geometric moiré
E_t^{super}	Envelope function (modulation of super-fringes) of time-average geometric moiré
F	Intensity of the image after filtering
I_1	Intensity of moiré grating in the state of equilibrium
I_2	Intensity of moiré grating in a deformed state
I_{d}	Intensity of double-exposure geometric moiré
$\bar{I}_{\mathrm{d}}$	Negative copy of the double-exposure geometric moiré image
$I_{\mathrm{d}}^{\mathrm{super}}$	intensity of super-moiré of double-exposure geometric moiré
I_t	Intensity of time-average geometric moiré
$\bar{I}_t$	Negative copy of the time-average geometric moiré image
$I_{\mathrm{t}}^{\mathrm{super}}$	Intensity of super-moiré of time-average geometric moiré
J_0	Zero-order Bessel function of the first kind
k	Constant
m	Positive integer
n	Integer
N	Order of a super-fringe
r_n	nth root of the zero-order Bessel function of the first kind
t	Time
tanh	Hyperbolic tangent (classical sigmoidal function)
T	Time of exposure
u	Displacement from the state of equilibrium
x	Coordinate
x^*	Centre of the super-fringe
Δx	Offset
y	Coordinate

Introduction

Geometric moiré [1, 2] is a classical optical experimental technique based on analysis of visual patterns produced by superposition of two regular gratings that geometrically interfere. Examples of gratings are equispaced parallel lines, concentric circles, radial lines [3–5]. The gratings can be superposed by double-exposure photography, by reflection, by shadowing, or by direct contact [6, 7]. Moiré patterns are used to measure variables such as displacements, rotations, curvature, and strain throughout the viewed area. In-plane moiré is typically conducted with gratings of equispaced, parallel lines [8].

The fringe derivative (in finite form) is the difference of two fringe orders over a specific distance.

Thus the displacement derivatives can be estimated simply, by measuring the fringe spacing in moiré patterns in the x and y directions and dividing those values into the pitch of the grating. An alternative is to generate super-moiré, or moiré-of-moiré patterns from the initial moiré patterns [1]. If a fringe pattern is duplicated photographically and the negative copy is laid on the original copy, offset by a specific distance, the fringes of the two copies will also interfere (just as the grating lines interfere) to form a super-moiré pattern [1, 9–11]. The new super-fringe pattern will represent the difference of the original fringes at every point in the field. If the offset is a linear shift in one direction (without rotation), the super-fringes will be proportional to the fringe difference per unit shift, in the direction of the shift. To avoid fractioning of the fringe orders, and in order to eliminate the original grating, the offset should be an integral number of pitches [1, 9].

Double-exposure geometric moiré techniques can be extended to time-average geometric moiré methods when the moiré grating is formed on the surface of elastic oscillating structure and time averaging techniques are used for the formation of patterns of fringes [12]. Dynamic displacements can be estimated from the time-average fringes, whereas the fringe order no longer represents the displacement by an integer number of pitches; the intensity of the time-averaged moiré pattern is governed by mathematical relationships comprising zero-order Bessel function of the first kind [13].

A variety of experimental techniques are used for the determination of strain fields from moiré patterns. Typically, the phase distribution of the fringes is extracted from digitised moiré patterns and then the unwrapped phase maps are numerically differentiated [14]. Alternatively, super-moiré of double-exposure geometric moiré is a classical experimental technique widely applied in different areas of optical engineering [1] and used for the determination of strain fields directly from the superposed fringe patterns.

Then the following question arises. Is it possible to apply super-moiré techniques (geometrical differentiation) for time-average geometric moiré? Will any super-fringes form if a negative copy of a time-average geometric moiré image is laid with an offset onto the original copy of the image (subtractive superimposition)? And finally, the most important question – if super-moiré fringes will occur, how can they be interpreted? This paper tries to find answers to the preceding questions and to show that time-average geometric super-moiré techniques can be successfully applied for the analysis of vibrating elastic structures.

One-dimensional Example

Initially, a one-dimensional example is analysed for simplicity. Moiré grating on the surface of a one-dimensional structure in the state of equilibrium can be interpreted as a harmonic function [1, 15, 16]:

$$I_1(x) = \cos^2\left(\frac{\pi}{\lambda}x\right), \tag{1}$$

where λ is the pitch of the grating. Such continuous function is well applicable for digital image processing in virtual computational environments [16]. Numerical value 0 of the function in Equation (1) corresponds to black colour; 1 – to white colour; all intermediate values – to grayscale intensity levels. The grating of one-dimensional structure in a deformed state can be interpreted as follows [12]:

$$I_2(x) = \cos^2\left(\frac{\pi}{\lambda}(x - u(x))\right), \tag{2}$$

where function $u(x)$ defines the displacement from the state of equilibrium at point x.

Intensity of double-exposure geometric moiré I_d (superposition of the gratings in the state of equilibrium and in the deformed state) can be expressed like an arithmetic mean of Equation (1) and Equation (2):

$$\begin{aligned} I_\mathrm{d}(x) &= \frac{1}{2}\left(\cos^2\left(\frac{\pi}{\lambda}x\right) + \cos^2\left(\frac{\pi}{\lambda}(x - u(x))\right)\right) \\ &= \frac{1}{2} + \frac{1}{2}\cos\left(\frac{2\pi}{\lambda}\left(1 - \frac{u(x)}{2x}\right)x\right)\cos\left(\frac{\pi}{\lambda}u(x)\right). \end{aligned} \tag{3}$$

The centres of the fringes are located at such values of x where the branches of the envelope function of the beatings

$$\frac{1}{2} \pm \frac{1}{2}\cos\left(\frac{\pi}{\lambda}u(x)\right)$$

intersect [12]:

$$u(x) = \lambda\left(n - \frac{1}{2}\right). \tag{4}$$

Alternatively, time-averaging techniques can be applied for the analysis of fringes produced by a grating formed on the surface of vibrating elastic one-dimensional structure. Then the carrier fringes are contrast modulated and the intensity of time-average geometric moiré image I_t can be described as [13]:

$$\begin{aligned} I_\mathrm{t}(x) &= \lim_{T\to\infty}\frac{1}{T}\int_0^T \cos^2\left(\frac{\pi}{\lambda}(x - u(x)\sin(\omega t - \varphi))\right)\mathrm{d}t \\ &= \frac{1}{2} + \frac{1}{2}\cos\left(\frac{2\pi}{\lambda}x\right)J_0\left(\frac{2\pi}{\lambda}u(x)\right), \end{aligned} \tag{5}$$

where T – time of exposure; ω and φ – angular frequency and phase of structural vibrations around the state of equilibrium, respectively; J_0 – zero-order Bessel function of the first kind. It can be noted that $u(x)$ now defines not static displacement, but the amplitude of dynamic displacement. The centres of time-average fringes are located at such values of x where the branches of the envelope function

$$\frac{1}{2} \pm \frac{1}{2} J_0\left(\frac{2\pi}{\lambda} u(x)\right)$$

intersect:

$$u(x) = \frac{\lambda}{2\pi} r_n, \tag{6}$$

where r_n is the nth root of J_0.

Super-moiré of Double-exposure Geometric Moiré

Lets assume that the offset is

$$\Delta x = \lambda n, \quad n = 1, 2, \ldots \tag{7}$$

and the negative copies of the geometric moiré images are defined as follows:

$$\begin{aligned} \bar{I}_\mathrm{d}(x) &= 1 - I_\mathrm{d}(x) \\ \bar{I}_\mathrm{t}(x) &= 1 - I_\mathrm{t}(x). \end{aligned} \tag{8}$$

Then, if the offset is equal to an integer number of pitches, super-moiré of double-exposure geometric moiré (subtractive superimposition) takes the following form:

$$\begin{aligned} I_\mathrm{d}^{\mathrm{super}}(x) &= \frac{1}{2}\left(I_\mathrm{d}(x) + \bar{I}_\mathrm{d}(x - \lambda n)\right) \\ &= \frac{1}{2} + \frac{1}{4}\left(I_2(x) - I_2(x - \lambda n)\right) \\ &= \frac{1}{2} + \frac{1}{4}\sin\left(\frac{\pi}{\lambda}\left(2x - (u(x) + u(x - \lambda n))\right)\right) \\ &\quad \times \sin\left(\frac{\pi}{\lambda}\left(u(x) - u(x - \lambda n)\right)\right). \end{aligned} \tag{9}$$

It can be noted that the original grating is eliminated from the moiré of moiré image. In this case, the envelope function characterising the modulation of super-fringes takes the following form:

$$E_\mathrm{d}^{\mathrm{super}}(x) = \frac{1}{2} \pm \frac{1}{4}\sin\left(\frac{\pi}{\lambda}\left(u(x) - u(x - \lambda n)\right)\right). \tag{10}$$

The centres of the super-fringes can be obtained from the equality $E_\mathrm{d}^{\mathrm{super}}(x) = 1/2$, which is satisfied when

$$u(x) - u(x - \lambda n) = \lambda N, \quad N = 0, \pm 1, \pm 2, \ldots \tag{11}$$

where N is the order of the super-fringe.

In general, the relationship between the derivative of the displacement from the status of equilibrium, the order of the super-fringe, the offset and the pitch of grating can be obtained dividing Equation (11) by Δx:

$$\frac{u(x) - u(x - \Delta x)}{\Delta x} = \frac{\lambda}{\Delta x} N, \quad N = 0, \pm 1, \pm 2, \ldots \tag{12}$$

If the displacement from the status of equilibrium is a linear function [$u(x) = kx$] and the offset is an integer number of pitches, the super-fringes are not formed (Figure 1E).

If the displacement from the status of equilibrium is a non-linear function (the offset is still an integer number of pitches) the super-fringes are formed (Figure 2E) and carry information about the derivative of displacement. Figure 2C clearly shows that the density of ordinary moiré fringes decreases when x increases – this is due to the shape of harmonic function $u(x) = A \sin(kx)$ in the first quarter of its period $0 \le x \le \pi/2k$. The density of fringes in Figure 2E is (on the contrary) higher at the right side

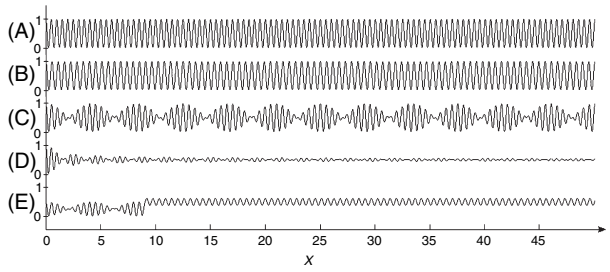

Figure 1: Formation of fringes when $u(x) = kx$: (A) $I_1(x)$; (B) $I_2(x)$; (C) $I_\mathrm{d}(x)$; (D) $I_\mathrm{t}(x)$; (E) $I_\mathrm{d}^{\mathrm{super}}(x)$ at $\lambda = 0.5$; $k = 0.12$; $\Delta x = 18\lambda$

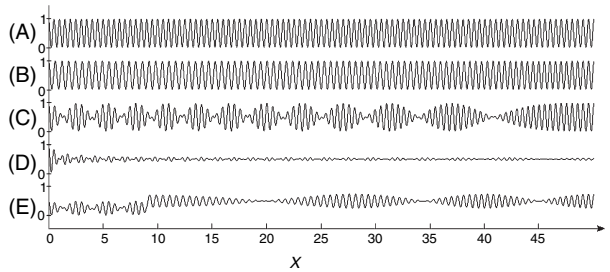

Figure 2: Formation of fringes when $u = A \cdot \sin(kx)$: (A) $I_1(x)$; (B) $I_2(x)$; (C) $I_\mathrm{d}(x)$; (D) $I_\mathrm{t}(x)$; (E) $I_\mathrm{d}^{\mathrm{super}}(x)$ at $\lambda = 0.5$; $A = 6$; $k = \pi/100$; $\Delta x = 18\lambda$

of the interval because of the shape of the cosine function [the derivative of $u(x)$].

Super-moiré of Time-average Geometric Moiré

In this case, the intensity of illumination will take the following form:

$$I_t^{super}(x) = \frac{1}{2}\left(I_t(x) + \bar{I}_t(x-\Delta x)\right) = \frac{1}{2} + \frac{1}{4}\cos\left(\frac{2\pi}{\lambda}x\right)\left(J_0\left(\frac{2\pi}{\lambda}u(x)\right) - J_0\left(\frac{2\pi}{\lambda}u(x-\lambda n)\right)\right). \quad (13)$$

Then, the envelope function of the produced image will be:

$$E_t^{super}(x) = \frac{1}{2} \pm \frac{1}{4}\left(J_0\left(\frac{2\pi}{\lambda}u(x)\right) - J_0\left(\frac{2\pi}{\lambda}u(x-\lambda n)\right)\right). \quad (14)$$

A super-fringe will be formed at such a point x^* in the vicinity of which the value of the envelope function is close to 1/2. In other words, a super-fringe will be located at such x where:

$$\forall x \in [x^*-\delta; x^*+\delta] : \frac{1}{4}\cdot\left|J_0\left(\frac{2\pi}{\lambda}u(x)\right) - J_0\left(\frac{2\pi}{\lambda}u(x-\lambda n)\right)\right| < \varepsilon, \quad (15)$$

where ε and δ are small positive numbers. The centre of the super-fringe can be found from the following equation:

$$J_0\left(\frac{2\pi}{\lambda}u(x^*)\right) - J_0\left(\frac{2\pi}{\lambda}u(x^*-\lambda n)\right) = 0. \quad (16)$$

The condition in Equation (15) will be satisfied when the values of functions

$$J_0\left(\frac{2\pi}{\lambda}u(x)\right) \quad \text{and} \quad J_0\left(\frac{2\pi}{\lambda}u(x-\lambda n)\right)$$

will coincide in some small interval around x^*. Such effect is illustrated in Figure 3.

It can be noted that the zero-order Bessel function of the first kind is almost a periodic function if only the surroundings of the function's roots are considered (Figure 4; Table 1):

$$J_0(x \in [r_{m+2N} - \delta \le r_{m+2N} \le r_{m+2N} + \delta]) \approx J_0(x \in [r_m - \delta \le r_m \le r_m + \delta]), \quad (17)$$

where r_i – ith root of the zero-order Bessel function of the first type; $m = 1, 2,\ldots$; $N = 0, \pm1, \pm2,\ldots$; $m + 2N \ge 1$. In the explicit form:

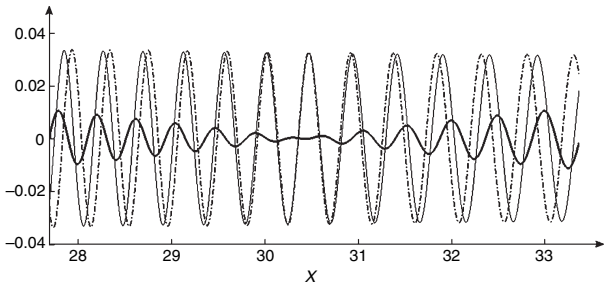

Figure 3: $J_0\left(\frac{2\pi}{\lambda}u(x)\right)$ – thin solid line; $J_0\left(\frac{2\pi}{\lambda}u(x-\Delta x)\right)$ – dash-dotted line; $\frac{1}{4}\left(J_0\left(\frac{2\pi}{\lambda}u(x)\right) - J_0\left(\frac{2\pi}{\lambda}u(x-\Delta x)\right)\right)$ – thick solid line at $\lambda = 0.05$; $u = A \cdot \sin(kx)$; $A = 6$; $k = \pi/100$; $\Delta x = 18\lambda$

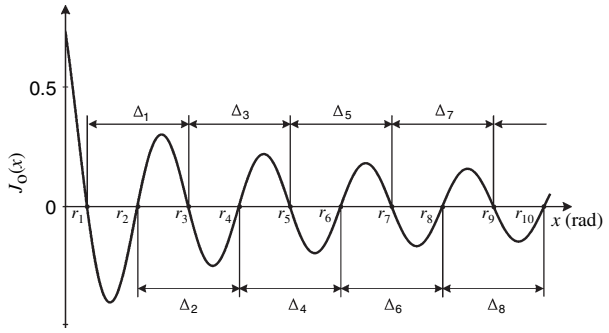

Figure 4: Roots of $J_0(x)$

Table 1: Distances between the roots of the zero order Bessel function of the first kind $\Delta_i = r_{i+2} - r_i$, $i = 1, 2,\ldots$

i	$\Delta_i/2\pi$	i	$\Delta_i/2\pi$	i	$\Delta_i/2\pi$
1	0.994544	11	0.999908	21	0.999973
2	0.998133	12	0.999922	22	0.999975
3	0.999046	13	0.999933	23	0.999978
4	0.999418	14	0.999942	24	0.999979
5	0.999607	15	0.999949	25	0.999981
6	0.999717	16	0.999955	26	0.999982
7	0.999786	17	0.999960	27	0.999984
8	0.999833	18	0.999964	28	0.999985
9	0.999866	19	0.999967	29	0.999986
10	0.999890	20	0.999971	30	0.999987

$$r_{m+2N} - r_m \approx 2\pi N. \quad (18)$$

So, if $(2\pi/\lambda)u(x^*-\Delta x)$ is in the surrounding of r_m, the equality (16) will be satisfied if and only if $(2\pi/\lambda)u(x^*)$ is in the surrounding of r_{m+2N}, where N is the order of a super-fringe; $N = 0, \pm1, \pm2,\ldots$ But then,

$$u(x^*) - u(x^* - \Delta x) = \frac{\lambda}{2\pi}(r_{m+2N} - r_m) \approx \lambda N. \quad (19)$$

This is an unexpected result (compare with Equation (11)). The density of ordinary moiré fringes in time-average geometric moiré images is almost double if compared to the density of fringes in double-

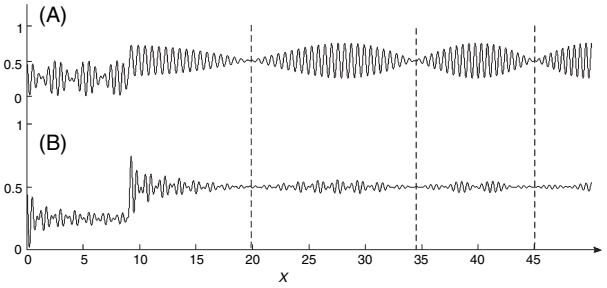

Figure 5: Super-moiré images: (A) $I_{\mathrm{d}}^{\mathrm{super}}(x)$; (B) $I_{\mathrm{t}}^{\mathrm{super}}(x)$ at $\lambda = 0.5$; $u = A \cdot \sin(kx)$; $A = 6$; $k = \pi/100$; $\Delta x = 18\lambda$

exposure geometric moiré images for the same values of dynamic and static displacements [12]. But the super-fringes generated by both methods almost coincide.

This effect is illustrated in Figure 5. The centers of super-fringes generated by super-moiré of double-exposure geometric moiré and super-moiré of time-average geometric moiré practically coincide. This leads to an important conclusion that geometric differentiation techniques can be applied for images generated by time-average geometric moiré. Moreover, the generated super-fringes carry the same physical information as super-fringes generated by moiré of double-exposure geometric moiré, and ordinary fringe counting techniques [1] can be used for the determination of the derivatives of displacements.

Unfortunately, there does not exist a specific offset for time-average moiré images which could eliminate the original grating in the state of equilibrium. Therefore the super-fringes in time-average images are not so clearly expressed if compared to super-fringes generated from double-exposure images. Nevertheless, application of digital image filtering techniques can help to identify super-fringes of higher orders what is demonstrated in the next section.

Super-fringe Patterns for a Vibrating Cantilevered Plate

A grating is formed on the surface of cantilevered elastic plate performing in-plane oscillations. Initially, natural eigenshapes of the structure are calculated using numerical finite element formulations [17]. The deformed grating on the surface of the structure at the status of maximum deformation (according to the second eigenshape) is plotted using numerical techniques described in detail in [16]. The image of the plate in the state of equilibrium is superposed with the image in the state of maximum

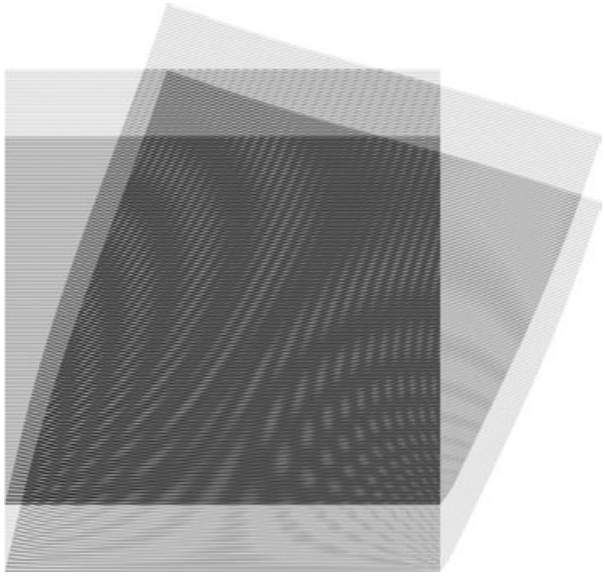

Figure 6: Double-exposure super-fringes, ordinary fringes and grating lines intertwined

deformation producing a pattern of double-exposure moiré fringes. Then this image is superposed with itself, offset by a certain distance in the direction orthogonal to the grating lines in the status of equilibrium. The produced image is presented in Figure 6. It can be noted that the offset is performed without the inversion of the image, so though the offset is equal to an integer number of pitches, the original grating is still visible. Digital image filtering techniques help highlight the super-fringes (Figure 7).

Next, time-averaged image of vibrating cantilevered plate is constructed using techniques described in detail in [12]. Then the produced time-averaged image is superposed with itself, offset by the same distance as in the previous experiment (Figure 8). As the intensity of time-averaged ordinary fringes is

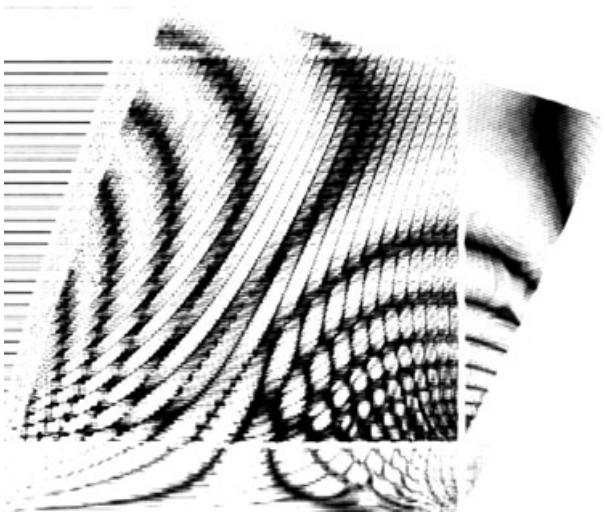

Figure 7: Filtered pattern of double-exposure super-fringes

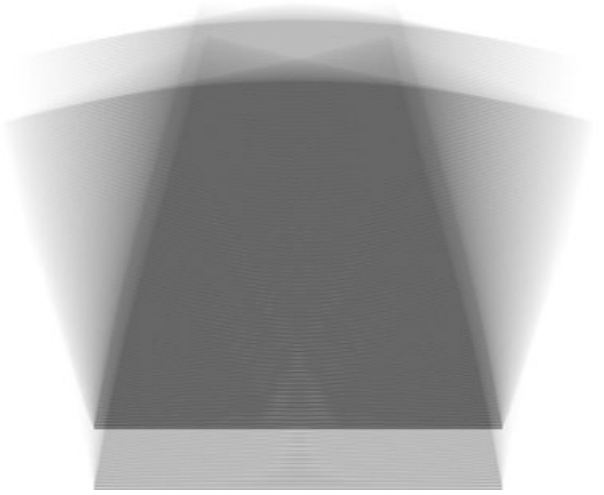

Figure 8: Time averaged super-fringes, ordinary fringes and grating lines intertwined

much lower compared with double-exposure fringes [13], it is quite natural to expect that time-averaged super-fringes would be hardly visible. Anyway, digital image filtering techniques enable clear reconstruction of the super-fringes in the time-averaged image (Figure 9).

Special digital image filtering techniques are to be used for sharpening the pattern of time-average super-fringes. The intensity of the digital image is equal to 0.5 at the centres of the super-fringes. Therefore, the digital image must be darkened where the intensity is around 0.5 and must be brightened elsewhere. Moreover, such transformation of the intensity levels must be smooth in order to avoid artificial boundary lines in the filtered image. We propose to use the following continuous representation:

$$F(I(x,y)) = \tanh^2(k(I(x,y) - 0.5)) \quad (20)$$

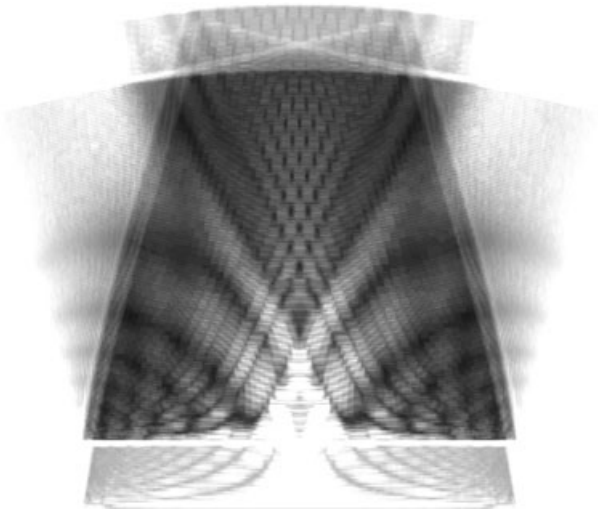

Figure 9: Filtered pattern of time-averaged super-fringes

where F is the intensity of the image after filtering; $I(x, y)$ is the intensity at a point (x, y) in the original image; tanh is hyperbolic tangent (classical sigmoidal function) and k is the parameter defining the depth of darkening of the digital image around $I = 0.5$. At $k < 1$, the whole image is darkened, but at higher values of k the produced filter characteristics are well suited for our application (Figure 10). It can be noted that parameter value $k = 50$ was used for producing digitally filtered image in Figure 9. Finally, it can be stressed that all experimental results presented in Figures 6–9 are produced and validated numerically in virtual computational environment [16].

Concluding Remarks

Geometric differentiation is a classical optical technique applicable for experimental identification of in-plane displacement derivatives from the patterns of moiré fringes. This paper shows that geometric differentiation can be also applied for identification of displacement derivatives from patterns of time-averaged moiré fringes. This fact is rather astonishing. The patterns of time-averaged moiré fringes are produced by continuous exposure of the vibrating structures surfaces of which are coated with moiré gratings. The generated fringes do not carry physical information on the static difference between the grating in the status of equilibrium and the grating in the deformed state. Time averaged fringes show the magnitude of dynamic displacement, which is harmonically varying in time. Moreover, the density of time-averaged fringes is almost double if compared to the density of fringes in double-exposure moiré for the same magnitudes of dynamic and static displacements. Therefore, it is quite unexpected that super time-averaged moiré fringes carry almost the same physical information on the magnitude of derivatives of dynamic displacements compared with double-exposure super-fringes.

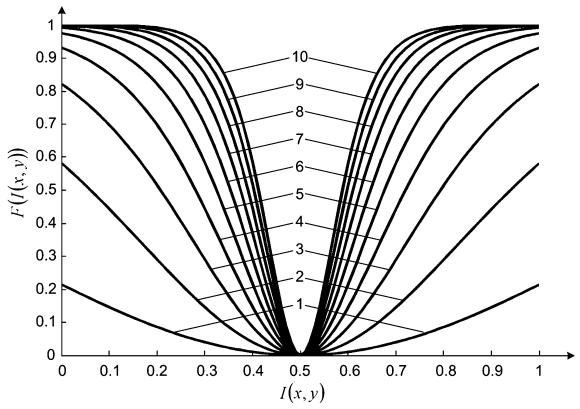

Figure 10: Digital filter characteristic at $k = 1, 2,\ldots,10$

The paper shows that geometric differentiation can be effectively applied for patterns of time-averaged moiré fringes. The fact that digital image filtering techniques are required for identification of time-averaged super-fringes does not lessen the practical value of the proposed method. It can be noted that the presented analysis is based on ideal mathematical and numerical simulation and serves as a theoretical insight into the complexity of time-average super-fringes. But successful congruence between theoretical and experimental analysis of ordinary time-average fringes in the previous studies anticipates also a good correlation between theoretical and experimental analysis of super-fringes, though experimental validation of the proposed technique is definitely an object of future research.

REFERENCES

1. Kobayashi, A. S. (1993) *Handbook on Experimental Mechanics*, 2nd edn. SEM, Bethel.
2. Post, D., Han, B. and Ifju, P. (1997) *High Sensitivity Moiré: Experimental Analysis for Mechanics and Materials*. Springer Verlag, Berlin.
3. Schultheisz, C. R. and Knauss, W. G. (1994) The governing equations of moiré interferometry II. Gratings at ±45° to the measurement axes. *Opt. Lasers Eng.* **20**, 283–293.
4. Verleysen, P. and Degrieck, J. (2004) Experimental investigation of the deformation of Hopkinson bar specimens. *Int. J. Impact Eng.* **30**, 239–253.
5. Liu, C. M. and Chen, L. W. (2004) Digital atomic force microscope moiré method. *Ultramicroscopy* **101**, 173–181.
6. Dai, F. L. and Wang, Z. Y. (1999) Geometric micron-moiré. *Opt. Lasers Eng.* **31**, 191–198.
7. Huimin, X., Guotao, W., Fulong, D., Guangjun, Z., Xingfu, L., Fangju, Z. *et al.* (1998) The dynamic deformation measurement of the high speed heated LY12 aluminium plate with moiré interferometry. *J. Mater. Process. Technol.* **83**, 159–163.
8. Field, J. E., Walley, S. M., Proud, W. G., Goldrein, H. T. and Siviour, C. R. (2004) Review of experimental techniques for high rate deformation and shock studies. *Int. J. Impact Eng.* **30**, 725–775.
9. Keren, E. and Kafri, O. (1983) A geometric approach for mapping of derivatives. *Comp. Phys. Commun.* **29**, 109–112.
10. Dally, J. W. and Riley, W. F. (1991) *Experimental Stress Analysis*, 3rd edn. McGraw-Hill, New York.
11. Parks, V. J. and Durelli, A. J. (1966) Moire patterns of partial derivatives of displacement components. *J. Appl. Mech.* **E33**, 901–906.
12. Ragulskis, M., Ragulskis, L. and Maskeliunas, R. (2004) Applicability of time average geometric moiré for vibrating elastic structures. *Exp. Tech.* **28**, 27–30.
13. Ragulskis, M., Maskeliunas, R., Ragulskis, L. and Turla, V. (2005) Investigation of dynamic displacements of lithographic press rubber roller by time average geometric moiré. *Opt. Lasers Eng.* **43**, 951–962.
14. Patorski, K. and Kujawinska, M. (1993) *Handbook on the Moiré Fringe Technique*. Elsevier, Amsterdam.
15. Ragulskis, M. and Ragulskis, L. (2004) Plotting isoclinics for hybrid photoelasticity and finite element analysis. *Exp. Mech.* **44**, 235–240.
16. Ragulskis, M., Palevicius, A. and Ragulskis, L. (2003) Plotting holographic interferograms for visualization of dynamic results from finite-element calculations. *Int. J. Numer. Methods Eng.* **56**, 1647–1659.
17. Bathe, K. J. (1982) *Finite Element Procedures in Engineering Analysis*. Prentice Hall, Englewood Cliffs, NJ.

